Fabrication of Micro/Nanofibrous Scaffolds using a Robotic Manipulator and Their Application for Tissue Engineering

Andrii Shynkarenko (andrii.shynkarenko@tul.cz)
Technicka Univerzita v Liberci https://orcid.org/0000-0003-0309-5618
Dekel Azulay
Afeka College of Engineering
Sarka Hauzerova
Technicka Univerzita v Liberci
Andrea Klapstova
Technicka Univerzita v Liberci
Michal Moucka
Technicka Univerzita v Liberci
Vera Jencova
Technicka Univerzita v Liberci
David Lukas
Technicka Univerzita v Liberci

Research

Keywords: microfibers, nanofibers, manipulator, fiber drawing, tissue engineering, crystallinity

Posted Date: November 25th, 2020

DOI: https://doi.org/10.21203/rs.3.rs-112972/v1

Abstract

Background: Nanofibrous materials currently find a wide range of medical and bioengineering applications including tissue-engineering scaffolds, sutures, and wound dressings. Recently, production of nanofibrous materials via Electrospinning has played a dominant role in this area. Here we introduce an alternative method, which we call the drawing method, which allows us to produce individual micro and nanofibers and to position them precisely into a two-dimensional network.

Results: The creation of such nano or micro fibrous networks is enabled thanks to a special arm-like robotic manipulator that we have designed, including its control system software. In this work we produced and tested microfibrous scaffolds of precise geometry made of two different biodegradable polymers: Polycaprolactone and Polylactide – Polycaprolactone copolymer. The microfibrous networks produced thereby were analyzed using a scanning electronic microscope and tested in vitro for cell adhesion and proliferation. The crystallinity of the resulting manufactured polymeric structures was evaluated using differential scanning calorimetry.

Conclusions: The mechanical drawing of individual microfibers presented in this article is a promising method to produce precisely oriented nano and microfibrous structures for technical as well as bioengineering applications. Our results indicate that the mechanical drawing of microfibers expands the possibilities for the preparation of tissue engineering scaffolds. Therefore, we believe that the range of applications of mechanical fiber drawing may soon expand.

1. Background

The production of polymer fibers with diameters ranging from hundreds of nanometres to tens of micrometres finds applications not only in tissue engineering [1], but also in nanoelectronics [2] and in the preparation of optical sensors [3]. These applications usually require the special production of regular and homogeneous one-dimensional (1D), two-dimensional (2D) or three-dimensional (3D) networks of uniform micro- and nanofibers. Therefore, the main challenge encountered in the production of such networks is the uniformity of fiber diameters and the requirement for their precise spatial arrangement [4].

A promising technology that meets such demands is the mechanical drawing of individual nanofibers. This technology has deep historical roots being firstly used by Boys in 1987 [5] to produce a torsion fiber to allow measurement of the gravitational constant. Boys attached a fragment of glass to the tail of an arrow, and heated it until a bead about the size of a pin's head had formed from the melted glass. Then the arrow, with the melted glass attached, was shot using a crossbow. The glassy bead remained behind on account of its inertia, but the arrow went forth. A tiny thread of glass was then drawn out between the tail of the arrow and the bead. The next evidence of the hidden potential of the drawing method is the work of Ondarçuhu and Joachim in 1998 [6]. They demonstrated that the limits of drawing fibers can be pushed down to the scale of nanometres. They also showed that nanofibers can be positioned precisely

on a surface during fabrication, and can then be cut or manipulated by an atomic force microscopy (AFM) tip.

The fiber drawing process involves the thinning dynamics of a polymeric solution or a melt, when a drop detaches from a capillary (additional description is shown on Figure 1 and is seen on the video in additional file drawing_1.mov and drawing_2.mov). The process of thinning the fiber follows different rules and dynamic scaling laws depending on the inertia, viscous stresses, or capillary forces involved [7]. The fiber drawing process may fail if a detached drop from a capillary breaks when reforming into a thinning thread. Two thinning regimes have been predicted and observed. The so-called viscocapillary regime at low Reynolds numbers [8] and the viscocapillary-inertial regime, when thinning significantly increases the inner fluid velocity [9].

Here we introduce a drawing process in which suspended fibers are fabricated by delivering a deposited polymer solution droplet using a pipette tip and drawing it in a state of liquid-solid transition using a robotic manipulator. The microfiber is then solidified by the rapid evaporation of the solvent due to the high surface area to volume ratio and the great difference in chemical potentials between a solvent inside the fiber and the ambient vapor of the solvent. The application of the manipulator significantly extends the ability of this technique, especially for two and three dimensional spatial scaffold geometries.

Fig. 1 Illustration of fiber creation by the fiber drawing method: Moving close to a surface (**A**), extrusion of a certain amount of polymer solution (**B**), creation of a fiber by the fast movement of a pipette to another location (**C**), touching the surface and fixation of the fiber (**D**).

2. Results

This section introduces the fiber morphology, differential scanning calorimetry analysis of mechanically drawn microfibers, and also biological testing of micro-fibrous structures including cell seeding and adhesion. To conduct our experiments, samples with parallel oriented fibers were prepared. The distance between single fibers was set to 0.015 mm. To increase the density of the structure, we repeated the process, applying more fibers on top of an existing layer. Each new layer was shifted by 1 micrometer in a direction perpendicular to the direction of drawing. In order not to disturb the layer already created, the length of each new layer was extended from 4 cm to 8 cm long (each layer was one cm longer than the previous). A schematic picture is shown in Figure 2 (A). Total amount of about 1000 individual fibers was reached (Fig. 2 B). They were fixed on special custom-made holders made from biocompatible Poly(methyl methacrylate) (PMMA) material (Fig. 2 C). The speed of manipulator's effector movement was set to 10 centimeters per second.

Fig. 2 The scheme of a dense structure of parallel microfibers formed by several subsequently created fiber layers (**A**). The real structure made by a layer of parallel fibers (**B**). A layer of parallel fibers clamped in a special custom made holder (**C**).

2.1 Morphological analysis of fibers

The morphology of the materials prepared was evaluated using electron microscopy and subsequent analysis of fiber diameters (Fig. 3, 4). The diameter of the fibers made of PCL and PLCL is comparable and achieves 4.288 ± 2.245 μm for PCL and 4.582 ± 1.719 μm for PLCL.

Fig. 3 SEM images of PCL (**A, C**) and PLCL (**B, D**): groups of microfibers (**A, B**), SEM images of detailed fiber morphology (**C, D**).

Fig. 4 Bar chart of fiber diameter distribution of PCL (**A**) and PLCL (**B**). Box plot of fiber diameter statistics for PCL and PLCL (**C**). Overview of fiber morphology characteristic values

2.2 Differential scanning calorimetry analysis

Melting enthalpy, melting temperature and degree of crystallinity for PCL and PLCL are presented in Table 1. The corresponding DSC spectra are introduced in Figure 5. Freshly prepared samples were subjected to analysis (approximately 20-30 minutes after fiber production)

Fig. 5 Differential scanning calorimetry analysis carried out on a range of temperatures from -20 to 100 for PCL and -40 to 130 for PCLC. DSC curves for 1st heating scans (heating rate of 3˚C/min) of (**A**) PCL, and (**B**) PLCL.

Table 1. Melting enthalpy, glass transition temperature, melting temperature and degree of crystallinity of PCL and PLCL at heating rate 10˚C/min.

	Enthalpy of fusion [Jg^{-1}]	Glass transition temperature [˚C]	Melting temperature [˚C]	Crystallinity [%]
PCL - first heating cycle	54.58	-	57.58	39.13
PCL - second heating cycle	51.06	-	55.07	36.60
PLCL - first heating cycle	3.61	18.11	77.28	0
PLCL - second heating cycle	0.00	18.54	-	0

2.3 Cell feeding and adhesion

PCL and PLCL fibers prepared using the drawing method were tested *in vitro* using 3T3 mouse fibroblasts. Cell behavior was monitored by microscopy (Fig. 6, 7). The preliminary results obtained show that the prepared materials allow cell adhesion and proliferation.

Fig. 6 Fluorescent microscopy of cells seeded on aligned fibers. Cells were stained with phaloidin-FITC (green) and DAPI (blue) : PCL after 1 (**A**), 3 (**B**) and 7 (**C**) days of incubation and PLCL fibers after 1 (**D**), 3 (**E**) and 7 (**F**) days of incubation. Scale bars: 50 μm.

Fig. 7 SEM images showing cells seeded on aligned PCL after 1. (**A**), 3. (**B**) and 7. (**C**) days of incubation and PLCL fibers after 1. (**D**), 3. (**E**) and 7. (**F**) days of incubation. Scale bar 20 μm.

Fluorescent microscope images as well as SEM images taken after 7 days show nearly confluent cell colonies. These colonies cover individual microfibers and, in several cases, also the gaps between them. The isotropy of individual cells is clearly evident from images taken at the first day (Fig. 6 A) a (Fig. 7 A D). Cell shapes are elongated in a direction parallel to the fibers' axis.

3. Discussion

The images on Figure 3 show that the prepared fibers do not have a smooth surface and numerous nanosized pores are visible on it. The surface morphology is similar for both evaluated materials, PCL and PLCL. This nanostructuring of the fiber surface is caused by solvent evaporation [10, 11, 12]. The diameters of the fibers prepared by our technology are therefore significantly smaller than the diameters of the fibers prepared by Strnadová [11]. They prepared fibers from a 12% (w/w) solution with a diameter of 5.80 ± 1.99 μm at the highest drawing speeds used.

Differential scanning calorimetry spectra of PCL reveals a decrease in the degree of crystallinity between the first and second heating cycles. A similar difference is seen in enthalpy values. The degree of crystallinity of PLCL is evidently close to zero. The normalized "melting" enthalpy in the first heating cycle is probably caused by the evaporation of residual solvent.

There is no significant difference between tested materials. Our results also show that the cells are growing in the direction of the fibers, so the prepared scaffolds support oriented cell growth. The cellular cultures on both PCL and PCL microfibers exhibit similar dynamic behavior.

4. Conclusions

The mechanical drawing of individual microfibers presented in this article is a promising method to produce precisely oriented nano and microfibrous structures for technical as well as bioengineering applications. As opposed to electrospinning, this method works without any electrically active parts and enables precise placement of the fibers created. A significant advantage of nanofiber formation using our manipulator is the ability to combine them according to strict geometry. Moreover, the materials may be prepared from biocompatible, degradable polymers. It enables, for example, the study of the behavior of cell cultures on conditioned scaffold geometry. Due to these properties, the material has great potential for use in tissue engineering, particularly for tissues where oriented cell growth is a key factor (e.g. nerve tissue). As an example of this, we have shown a promising application of parallel structures. Our apparatus has great potential because it enables the creation of microfibers from common polymeric

solutions. Subsequent testing suggested that our set-up also enables us to spin PCL microfibers from a polymeric melt. A suitable combination of changeable pipettes containing different types of polymer solutions/melts also enables the creation of composite micro-fibrous grids with several special properties such as biological, catalytic or sorption. The preliminary results of *in vitro* testing show that the prepared materials allow cell adhesion and proliferation. The robotic arm manipulator is very accessible and affordable, making it suitable to fill a great number of laboratory requirements. Therefore, we believe that the range of applications of mechanical fiber drawing may soon expand.

5. Materials And Methods

This section introduces the experimental equipment, the material used, a description of fiber morphology analysing and preparation of *in vitro* testing.

5.1 Experimental equipment

Manipulator. The manipulator we used for the mechanical drawing of fibers is based on the “Uarm swift pro” robotic arm (Fig. 8 A). It is an affordable, open-source robotic manipulator with four degrees of freedom and a maximum payload of half a kilogram. The manipulator enables the drawing of fibers by the movement of its arm between two arbitrarily selected points in 3D space. The polymer solution is extruded automatically from a micropipette at the tip of the robotic arm at the beginning of each drawing movement (Fig. 8 B). The fiber is created between the delivered droplet on the substrate and the polymer solution that remains on the pipette orifice. The robotic arm leads its fiber end to a substrate point determined by the control software. This process can be performed consistently over a great number of repetitions.

The idea of using a robotic arm for this application comes from an open-source project called OpenLH (an open Liquid-Handling System for creative experimentation with biology) from miLAB research laboratory [13]. The project has undergone deep alterations and improvements in both its mechanical and software aspects.

Extruder. A special effector for the robotic arm was designed for polymer extrusion (Fig. 8 B). It is based on the so-called positive displacement pipette (PDP) Microman from the company Gilson. The Microman pipette does not need an air cushion, as opposed to air displacement pipettes [14]. This technology offers a reduction of solvent evaporation and prevents cross contamination, since there is no direct contact between the substrate and the pipette. For operation with a robotic manipulator, we designed a custom-made construction and combined it with the original components. All necessary parts for connections and the installation of the manipulator were made using additive manufacturing technology based on the HP Jet Fusion 3D printer. The pipette tip could be updated with a special 3D printed ceramic [15] heater which was specially developed by us for this extruder (Fig. 8 C). As a result, our device can now use heat to change the rheological properties of polymeric melts and solutions. We conducted a series of experiments with PCL polymer by melting it instead of dissolving it in solvents and got promising results.

Fig. 8 General view of the manipulator and work surface (**A**). Effector of manipulator. Dosing pipette (**B**). Heater element for PDP tip (**C**).

User interface. We developed user-friendly software to allow every user to program this system to his or her needs, e.g., to change and combine algorithms and to use the manipulator for different, previously mentioned applications. The graphical user interface (GUI) is based on the uArm Python Software Development Kit (SDK) supplied by Ufactory, producer of the uArm.

Applications. The manipulator enables the fibers made from different polymer solutions. Such structures could also be used in nanoelectronics [2] or be applied as optical sensors [3]. Furthermore, the manipulator can be used in the fields of nanomaterials and biology for routine laboratory pipetting operations thanks to its highly accurate liquid dosing mechanism. The manipulator can also be used to good effect in the field of dip-coating, which is a popular way of creating thin film coated materials. Dip-coating involves the immersion of a substrate into a tank containing coating material, removing the piece from the tank, and allowing it to drain. The coated piece can then be dried by force-drying or baking. All these operations can be carried out by the robotic arm of the manipulator [16].

5.2 Polymer solution

Polymer solutions PCL (Mw 80,000, Sigma) and PLCL (PLC7015, Corbion), prepared with a concentration of 12% (w/w) in chloroform (Penta), were used to produce drawing fibers.

5.3 Fiber characterization

Fiber morphology was analyzed using pictures taken by a scanning electron microscope (SEM). Samples were sputter coated with gold (10nm) and then observed by SEM (Tescan, Vega 3 SB easy probe). Fiber diameter was measured using ImageJ software and then evaluated from a total of 100 measurements and shown in the form of a box plot.

5.4 Differential scanning calorimetry analysis

Processing - in our case mechanical fiber drawing – can have an impact on the initial crystallinity of PCL. The first heating cycle assesses the properties of the material in its post-production state, i.e., just after mechanical drawing of fibers. Heating the sample above its melt transition and the following cooling erases information about the fiber's technological history and imparts a normalized thermal profile upon the sample. The second heating cycle evaluates the inherent properties of the material [17]. Moreover, the degree of crystallinity affects the rate of biodegradation of polymeric materials. Therefore, it is important to study the relationship between the degree of crystallinity on one side and the material and technological parameters on another.

The crystallinity measurement was performed using a Mettler Toledo DSC1 calorimeter from -20°C to 100°C for PCL fibers and from -40°C to 130°C for PLCL fibers with a heating rate of 10°C/min. All

experiments were conducted in a nitrogen atmosphere. The degree of crystallinity was evaluated from equation (1) using melting enthalpy.

$$\chi_c = (\Delta H_{m1}/\Delta H_m^0) \times 100, \quad (1)$$

where ΔH_{m1} is the enthalpy of melting measured during the first heating cycle (Fig. 5 A black) and is the melting enthalpy of a pure PCL crystal (139.5 $J.g^{-1}$) (Fig. 5 A red) [18].

5.5 In vitro tests

Samples for *in vitro* testing were prepared as set of 1000 individual fibers fixed with a supporting ring designed to fit the cavities of a 24-well culture plate [11]. Prior to cell seeding, samples were sterilized in 70% ethanol for 30 minutes, then washed several times in PBS (phosphate buffer saline, pH 7.4) and given a final wash in a DMEM medium (Biosera). 3T3 mice fibroblasts (3T3 Swiss Albino, ATCC) were seeded at a concentration of 1.10^5 cells per well in 24-well plates. The cells were maintained in Dulbecco's modified eagle medium (DMEM, Biosera) and supplemented with fetal bovine serum (FBS, Biosera), glutamine (Biosera), and antibiotics Pen/Strep Amphotericin B (Lonza). The cells were cultured in an incubator at 37° C and 5% CO2, the medium was changed three times a week and the sixth passage were used for the in vitro experiments.

The samples were analyzed for cell behavior using florescence microscopy and scanning electron microscopy (SEM) on days 1, 3 and 7 after cell seeding. The samples processed for microscopy were fixed with 2.5% glutaraldehyde for 15 minutes. After the fixation of cells, the samples for fluorescent microscopy were rinsed in PBS and then permeabilised for 10 minutes in a solution of 0.1% BSA (Merck) and 0.1% Triton in PBS. Next, the cells were stained with DAPI (Merck) and phalloidin-FITC (Merck). After permeabilisation, the samples were washed with PBS and stained with phalloidin-FITC (1µg/ml) in for 30 minutes at room temperature. Then the samples were washed with PBS and stained with 0,1% DAPI for 10 minutes at room temperature. The samples were then analyzed with a fluorescence microscope (Nikon Eclipse Ti-e). Samples intended for SEM were rinsed in PBS and then dried with in an increasing concentration of ethanol (60%, 70%, 80%, 90%, 96% and 100%). After drying, the samples were fixed on targets, sputter-coated with a 10nm-thick layer of gold and analyzed by a scanning electron microscope (Tescan, Vega 3 SB easy probe).

Abbreviations

1D
One-dimensional
2D
Two-dimensional
3D

Three-dimensional
3T3
3-day transfer, inoculum 3 × 105 cells
AFM
Atomic Force Microscopy
BSA
Bovine Serum Albumin
DAPI
4',6-diamidino-2-phenylindole
DMEM
Dulbecco's Modified Eagle Medium
DSC
Differential Scanning Calorimetry
FBS
Fetal Bovine Serum
FITC
Fluorescein Isothiocyanate
GUI
Graphical User Interface
HP
Hewlett-Packard
PBS
Phosphate Buffer Saline
PCL
Polycaprolactone
PDP
Positive Displacement Pipette
PLCL
Polycaprolactone Copolymer
PMMA
Poly (methyl methacrylate)
SDK
Software Development Kit
SEM
Scanning Electronic Microscope

Declarations

- **Ethics approval and consent to participate**

Not applicable

- **Consent for publication**

Not applicable

- **Availability of data and materials**

Our developed control system software is available via a personal link:

http://www.ksa.tul.cz/getFile/id:4379

All measurement data, images and analysis from work can be provided upon request

- **Competing interests**

The authors declare that they have no competing interests

- **Funding**

This publication was written at Technical University of Liberec as part of the project “Development of a multifunctional robotic system for manipulation with nanostructures” with the support of the Specific University Research Grant SGS 21293, as provided by the Ministry of Education, Youth and Sports of the Czech Republic in the year 2019.

- **Authors' contributions**

All authors read and approved the final manuscript

- **Acknowledgements**

This publication was written at Technical University of Liberec as part of the project “Development of a multifunctional robotic system for manipulation with nanostructures” with the support of the Specific University Research Grant SGS 21293, as provided by the Ministry of Education, Youth and Sports of the Czech Republic in the year 2019. The authors also thank Luboš Běhalák, at the Technical University of Liberec, for his assistance with DSC analysis and the laboratory of rapid prototyping at The Institute for Nanomaterials, Advanced Technology and Innovation in Liberec. We also thank the miLAB research laboratory for inspiration with an open Liquid-Handling System for creative experimentation with bioengineering.

References

1. Prince E, Kumacheva E. Design and applications of man-made biomimetic fibrillar hydrogels. Nature Reviews Materials. 2019;4:99–115.

2. Wang X, Drew C, Lee S-H, Senecal KJ, Kumar J, Samuelson LA. Electrospun Nanofibrous Membranes for Highly Sensitive Optical Sensors. Nano Lett. 2002;2:1273–5.
3. Whitesides GM, Grzybowski B. Self-Assembly at All Scales. Science. 2002;295:2418–21.
4. Nain AS, Wong JC, Amon C, Sitti M. Drawing suspended polymer micro-/nanofibers using glass micropipettes. Appl Phys Lett. 2006;89:183105.
5. Boys CV. On the Production, Properties, and some suggested Uses of the Finest Threads. Proc Phys Soc London. 1887;9:8–19.
6. Ondarçuhu T, Joachim C. Drawing a single nanofibre over hundreds of microns. EPL. 1998;42:215.
7. Petit J, Riviere D, Kellay H, Delville J-P. Break-up dynamics of fluctuating liquid threads. Proceedings of the National Academy of Sciences. 2012;109:18327–31.
8. Papageorgiou DT. On the breakup of viscous liquid threads. Phys Fluids. 1995;7:1529–44.
9. Eggers J. Universal pinching of 3D axisymmetric free-surface flow. Phys Rev Lett. 1993;71:3458–60.
10. Megelski S, Stephens JS, Chase DB, Rabolt JF. Micro- and Nanostructured Surface Morphology on Electrospun Polymer Fibers. Macromolecules. 2002;35:8456–66.
11. Strnadová K, Stanislav L, Krabicová I, Sabol F, Lukášek J, Řezanka M, et al. Drawn aligned polymer microfibres for tissue engineering. Journal of Industrial Textiles. 2019;1528083718825318.
12. Yang A, Huang Z, Yin G, Pu X. Fabrication of aligned, porous and conductive fibers and their effects on cell adhesion and guidance. Colloids Surf B. 2015;134:469–74.
13. Gome G, Waksberg J, Grishko A, Wald IY, Zuckerman O. OpenLH: Open Liquid-Handling System for Creative Experimentation with Biology. Proceedings of the Thirteenth International Conference on Tangible, Embedded, and Embodied Interaction - TEI '19 [Internet]. Tempe, Arizona, USA: ACM Press; 2019 [cited 2019 Dec 1]. p. 55–64. Available from: http://dl.acm.org/citation.cfm?doid=3294109.3295619.
14. Le Rouzic E. Contamination-pipetting: relative efficiency of filter tips compared to Microman® positive displacement pipette. Nat Methods. 2006;3:III–V.
15. Kovalenko I, Ramachandran Y, Garan M. EXPERIMENTAL SHRINKAGE STUDY OF CERAMIC, DLP 3D PRINTED PARTS AFTER FIRING GREEN BODIES IN A KILN. MM SJ. 2019;2019:2767–71.
16. Faustini M, Louis B, Albouy PA, Kuemmel M, Grosso D. Preparation of Sol – Gel Films by Dip-Coating in Extreme Conditions. J Phys Chem C. 2010;114:7637–45.
17. Simon GP. Polymer Characterization Techniques and Their Application to Blends. Oxford: Oxford University Press; 2003.
18. Bagher AM, Reza BM. Polymer Optic Technology. Optics. 2015;4:1.

Figures

Figure 1

Illustration of fiber creation by the fiber drawing method: Moving close to a surface (A), extrusion of a certain amount of polymer solution (B), creation of a fiber by the fast movement of a pipette to another location (C), touching the surface and fixation of the fiber (D).

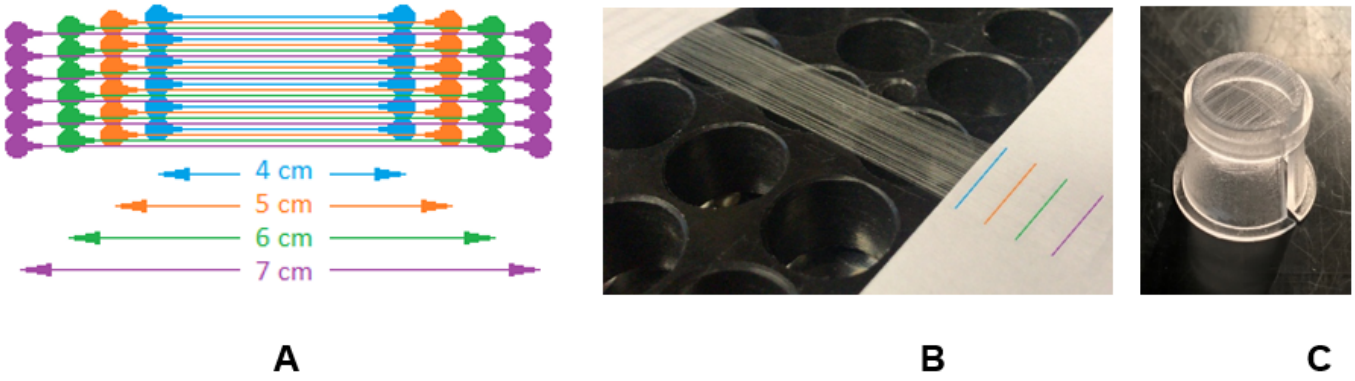

Figure 2

The scheme of a dense structure of parallel microfibers formed by several subsequently created fiber layers (A). The real structure made by a layer of parallel fibers (B). A layer of parallel fibers clamped in a special custom made holder (C).

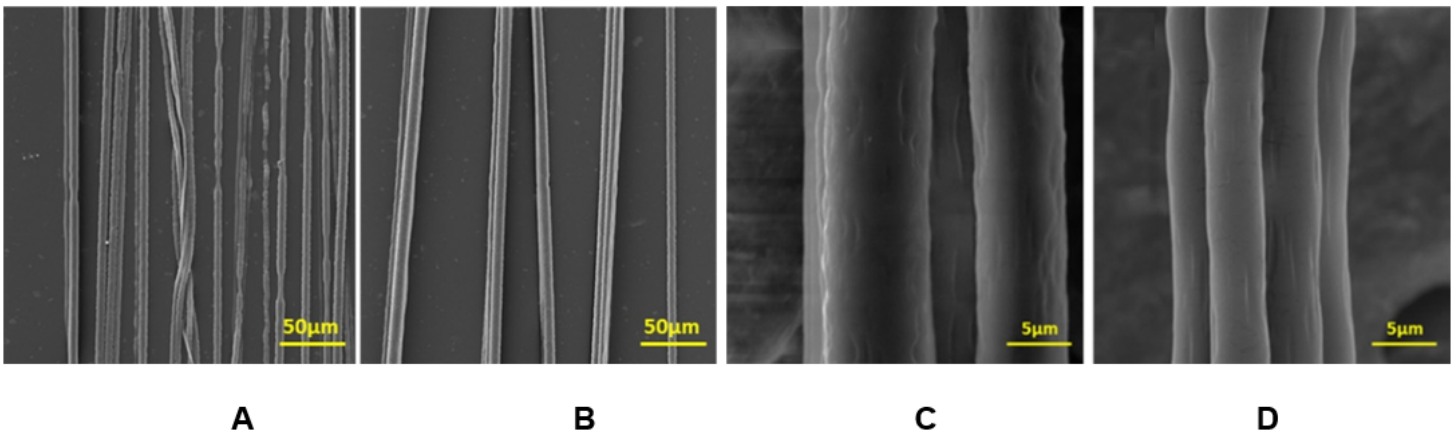

Figure 3

SEM images of PCL (A, C) and PLCL (B, D): groups of microfibers (A, B), SEM images of detailed fiber morphology (C, D).

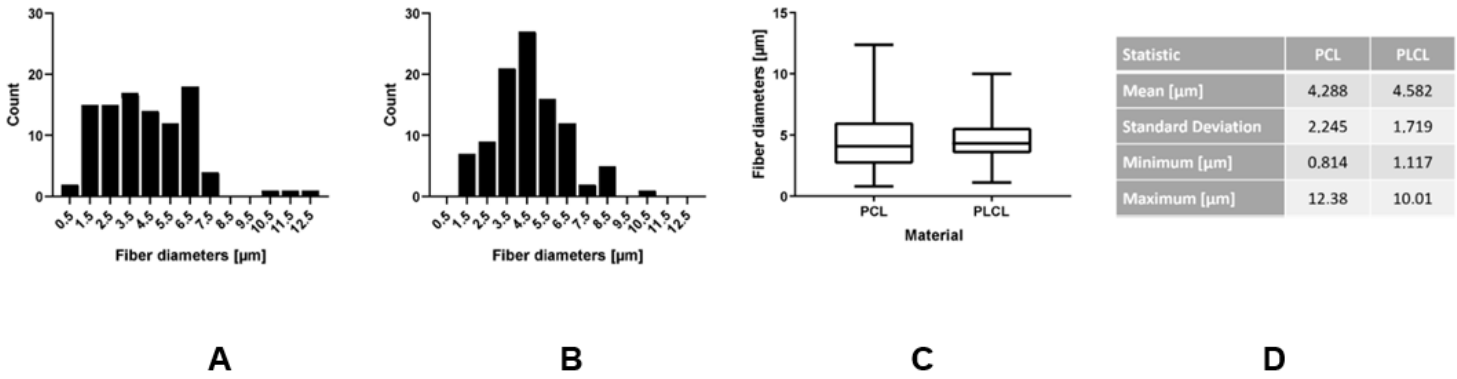

Statistic	PCL	PLCL
Mean [µm]	4.288	4.582
Standard Deviation	2.245	1.719
Minimum [µm]	0.814	1.117
Maximum [µm]	12.38	10.01

A B C D

Figure 4

Bar chart of fiber diameter distribution of PCL (A) and PLCL (B). Box plot of fiber diameter statistics for PCL and PLCL (C). Overview of fiber morphology characteristic values.

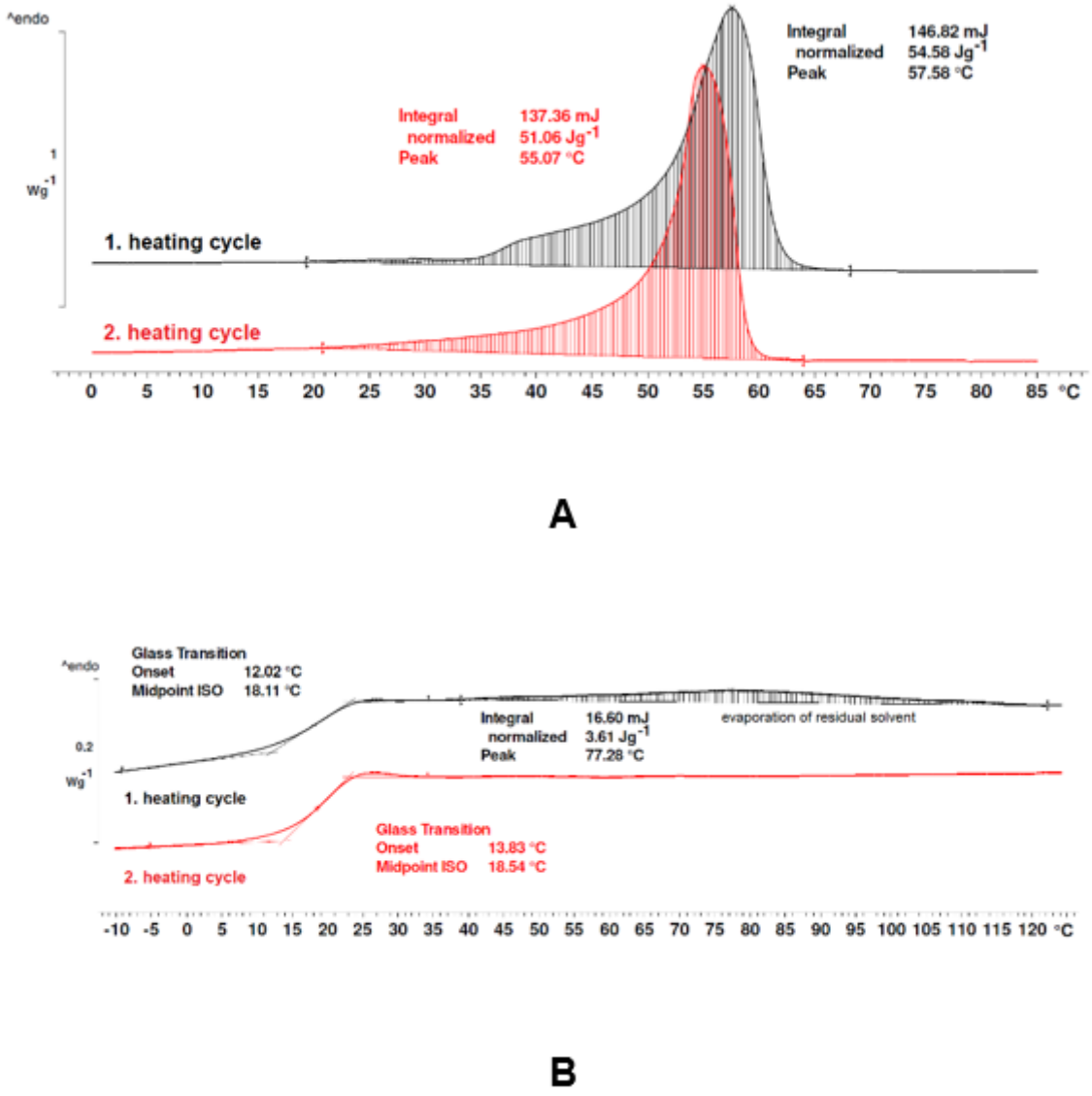

Figure 5

Differential scanning calorimetry analysis carried out on a range of temperatures from -20 to 100 for PCL and -40 to 130 for PCLC. DSC curves for 1st heating scans (heating rate of 3˚C/min) of (A) PCL, and (B) PLCL.

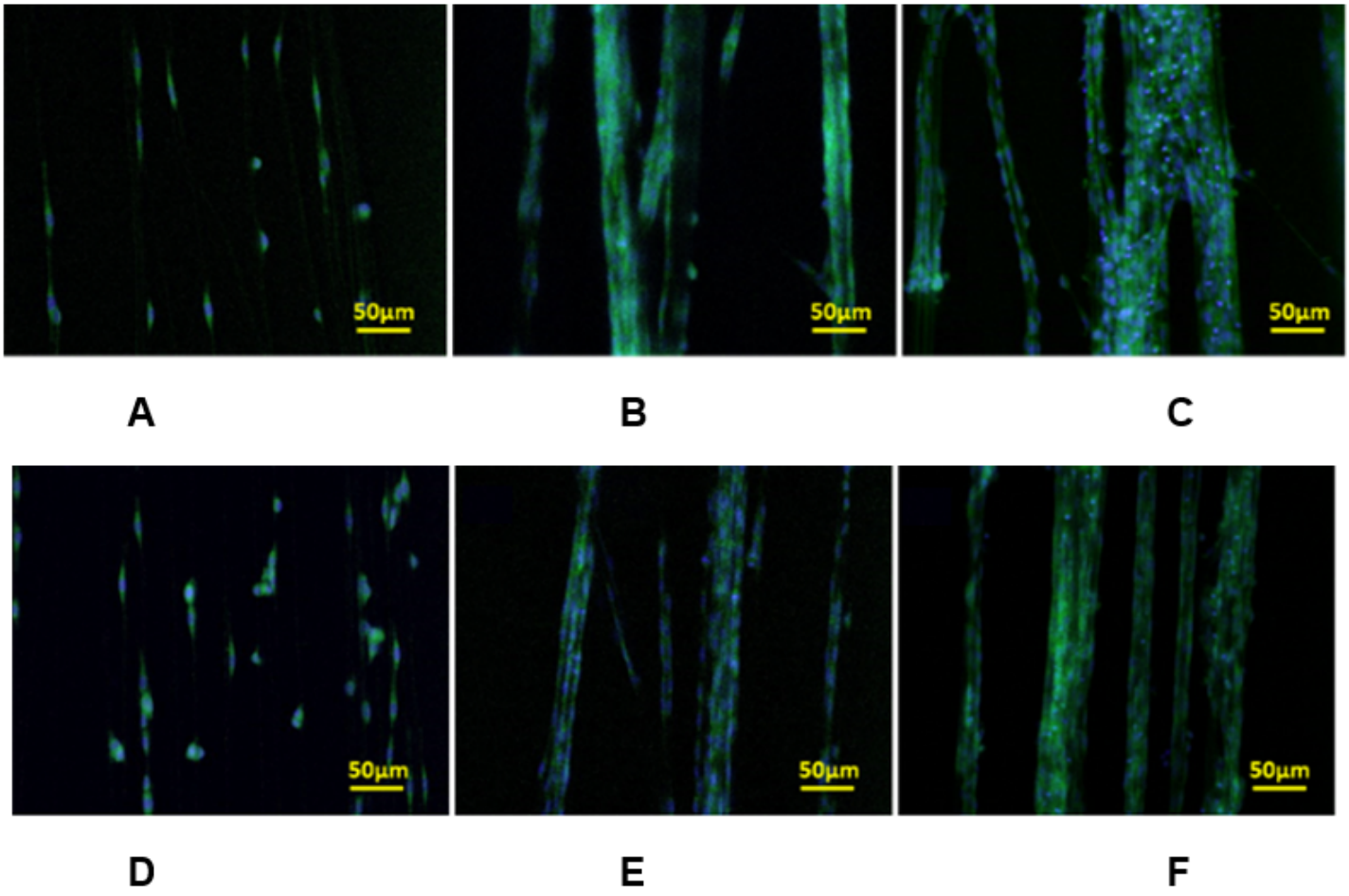

Figure 6

Fluorescent microscopy of cells seeded on aligned fibers. Cells were stained with phaloidin-FITC (green) and DAPI (blue) : PCL after 1 (A), 3 (B) and 7 (C) days of incubation and PLCL fibers after 1 (D), 3 (E) and 7 (F) days of incubation. Scale bars: 50 µm.

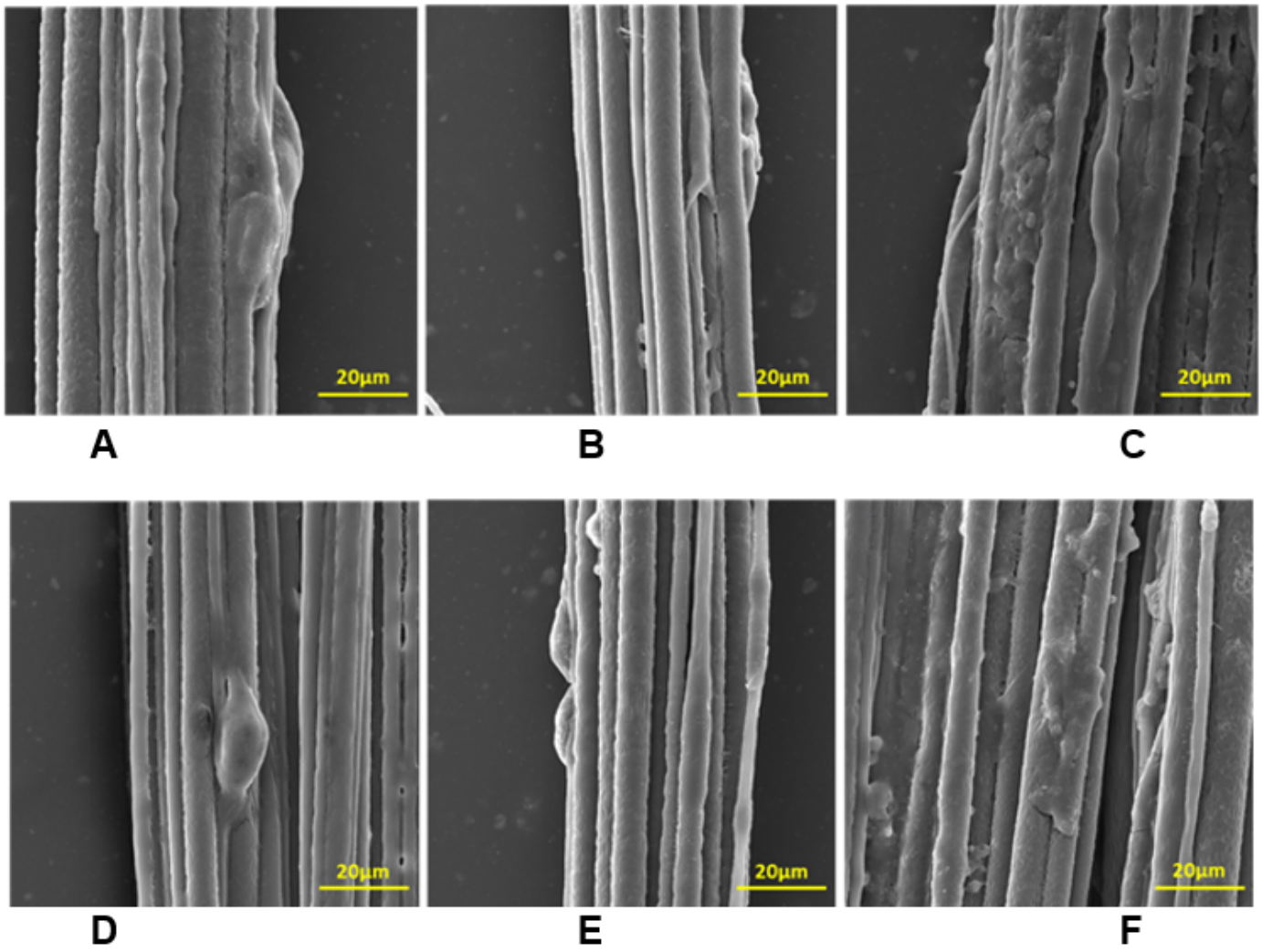

Figure 7

SEM images showing cells seeded on aligned PCL after 1. (A), 3. (B) and 7. (C) days of incubation and PLCL fibers after 1. (D), 3. (E) and 7. (F) days of incubation. Scale bar 20 µm.

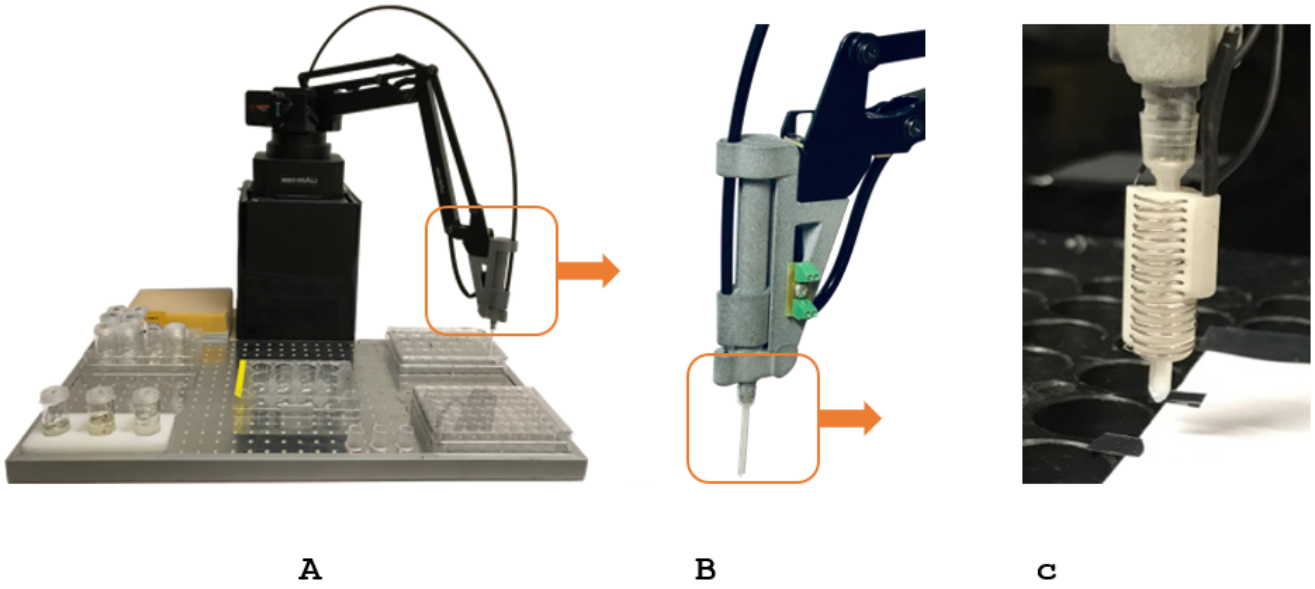

Figure 8

General view of the manipulator and work surface (A). Effector of manipulator. Dosing pipette (B). Heater element for PDP tip (C).

Supplementary Files

This is a list of supplementary files associated with this preprint. Click to download.

- GA.png
- drawing1.MOV
- drawing2.mov